Environmental Science & Technology

Article

pubs.acs.org/est

Enhanced Performance of Ceria-Based NO_x Reduction Catalysts by Optimal Support Effect

Junxiao Chen,[†,§] Yaxin Chen,[†,§] Meijuan Zhou,[†] Zhiwei Huang,[†] Jiayi Gao,[†] Zhen Ma,[†] Jianmin Chen,[†] and Xingfu Tang*[,†,‡]

[†]Institute of Atmospheric Sciences, Shanghai Key Laboratory of Atmospheric Particle Pollution & Prevention, Department of Environmental Science & Engineering, Fudan University, Shanghai 200433, China

[‡]Jiangsu Collaborative Innovation Center of Atmospheric Environment and Equipment Technology, Nanjing University of Information Science & Technology, Nanjing 210044, China

Supporting Information

ABSTRACT: CeO_2-based catalysts have attracted widespread attention in environmental-protection applications, including selective catalytic reduction (SCR) of NO by NH_3, and their catalytic performance is often intimately associated with the supports used. However, the issue of how to choose the supports of such catalysts still remains unresolved. Herein, we systematically study the support effect in SCR over CeO_2-based catalysts by using three representative supports, Al_2O_3, TiO_2, and hexagonal WO_3 (HWO), with different acidic and redox properties. HWO, with both acidic and reducible properties, achieves an optimal support effect; that is, CeO_2/HWO exhibits higher catalytic activity than CeO_2 supported on acidic Al_2O_3 or reducible TiO_2. Transmission electron microscopy and X-ray diffraction techniques demonstrate that acidic supports (HWO and Al_2O_3) are favorable for the dispersion of CeO_2 on their surfaces. X-ray photoelectron spectroscopy coupled with theoretical calculations reveals that reducible supports (HWO and TiO_2) facilitate strong electronic CeO_2−support interactions. Hence, the excellent catalytic performance of CeO_2/HWO is mainly ascribed to the high dispersion of CeO_2 and the optimal electronic CeO_2−support interactions. This work shows that abundant Brønsted acid sites and excellent redox ability of supports are two critical requirements for the design of efficient CeO_2-based catalysts.

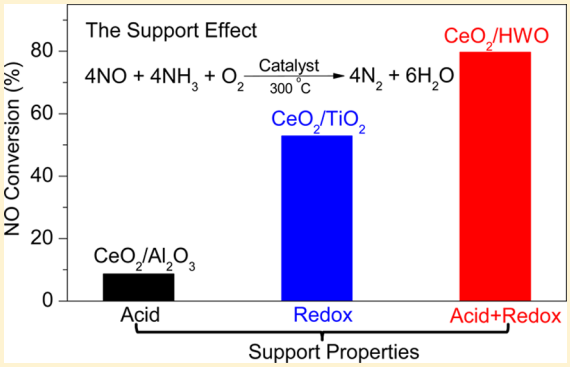

INTRODUCTION

Nitrogen oxides (NO_x) emitted from stationary and mobile sources have raised significant concern due to their great contribution to acid rain and photochemical smog.[1] Selective catalytic reduction (SCR) of NO_x with NH_3 is one of the most promising abatement technologies. V_2O_5-based catalysts have been used commercially for SCR,[2−4] but the toxicity of vanadium limits their widespread application. In response to increasingly stringent environmental regulations, it is desirable to develop environmentally benign catalysts to control NO_x emissions efficiently. CeO_2 is an environmentally friendly active component of such efficient catalysts for SCR,[5−7] owing to its excellent oxygen storage/release ability via the Ce^{4+}/Ce^{3+} redox cycle.[8,9]

Supports can influence the catalytic performance of CeO_2-based catalysts dramatically.[10−13] To rationally design efficient supports, a clear understanding of the SCR mechanism and the synergistic CeO_2−support effect is necessary. Eley−Rideal and Langmuir−Hinshelwood models are often used to describe the SCR mechanisms for CeO_2-based catalysts, and the adsorption and activation of NH_3 are regarded as two key steps in both models.[14] NH_3 that participates in the SCR reactions was found to be mostly adsorbed on Brønsted acid sites and subsequently activated.[15] Therefore, supports with abundant Brønsted acid sites and the ability to enhance the redox property of CeO_2 are favorable for NH_3 adsorption and activation. An excellent support can not only allow CeO_2 to be highly dispersed on the supports' surfaces but also induce synergistic CeO_2−support interactions. Supports with acidic properties, especially those with abundant Brønsted acid sites such as Al_2O_3[12,16] and WO_3,[17,18] are beneficial for the dispersion of CeO_2 nanoparticles with basic properties. Reducible supports such as TiO_2 and WO_3 are often used to provoke CeO_2−support interactions via redox reactions.[17−19] Thus, supports with both abundant acid sites and excellent redox properties should be ideal for the design of CeO_2-based catalysts for SCR, but a systematic study of support effect is still lacking.

Al_2O_3, TiO_2, and WO_3 with different acid and redox properties have been used to prepare CeO_2-based SCR catalysts.[16−20] For instance, CeO_2 supported on acidic Al_2O_3 achieved high SCR activity at 250−350 °C.[12] CeO_2/TiO_2 gave

Received: August 11, 2016
Revised: November 10, 2016
Accepted: December 2, 2016
Published: December 2, 2016

DOI: 10.1021/acs.est.6b04050
Environ. Sci. Technol. 2017, 51, 473−478

almost complete conversion of NO in a wide temperature window (200−400 °C) because of the strong CeO_2−TiO_2 interactions via the surface Ce−O−Ti bridging bonds.[19] Owing to the acid property and redox characteristics of WO_3, CeO_2/WO_3 showed extraordinary catalytic performance in SCR at 200−450 °C even at a high gas hourly space velocity (GHSV).[21] However, these catalysts were tested under quite different conditions, thus making the comparison of their intrinsic activities impossible. Therefore, it is desirable to distinguish the support effect under identical conditions to choose suitable supports for CeO_2-based catalysts.

In this work, we study the support effect in SCR over CeO_2-based SCR catalysts by using Al_2O_3, TiO_2, and hexagonal WO_3 (HWO) as representative supports (Scheme 1). The activities

Scheme 1. Illustration Showing the Design of CeO_2-based Catalysts with Three Representative Supports According to Acid and Redox Properties

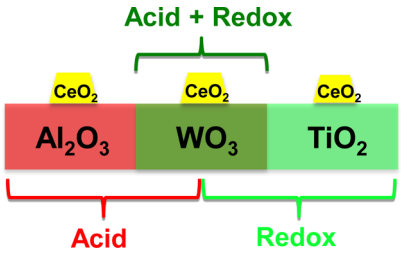

of these CeO_2-based catalysts were tested under the same conditions, and these catalysts were characterized by various techniques such as transmission electron microscopy (TEM), synchrotron X-ray diffraction (SXRD), X-ray photoelectron spectroscopy (XPS), and hydrogen temperature-programmed reduction (H_2-TPR). A conclusion on how to design efficient CeO_2-based SCR catalysts was then reached. This work could assist the design of improved SCR catalysts from the support effect point of view.

MATERIALS AND METHODS

Materials Preparation. HWO was prepared by a hydrothermal method.[22] Briefly, a solution composed of $(NH_4)_{10}W_{12}O_{41}$ (0.7 mmol), $(NH_4)_2SO_4$ (63.0 mmol), oxalic acid (23.3 mmol), and deionized water (80 mL) was sufficiently mixed, transferred to a 100 mL autoclave, and put into an oven at 180 °C for 12 h via rotary hydrothermal treatment. The obtained slurry was filtered, washed with deionized H_2O, and dried at 105 °C. CeO_2/MO_x (M = Al, Ti, or W) was prepared by precipitation: MO_x (2.00 g) was mixed with 50 mL of $CeCl_3$ (43 mM) solution, and 10 mL of $NH_3{\cdot}H_2O$ (2.5 wt %) solution was then added. The suspension was aged for 0.5 h and then centrifuged at 8500 rpm. The product was washed with deionized water three times, dried at 105 °C for 12 h, and calcined at 400 °C for 4 h.

Catalytic Evaluation. SCR was performed in a fixed-bed quartz reactor (i.d. = 8 mm) under atmospheric pressure. The mixed feed gas contained 500 ppm of NO, 500 ppm of NH_3, 3.0 vol % O_2, and balance N_2. The total flow rate was 1000 mL·min^{-1}. For each run, a certain amount of catalyst (40−60 mesh) was charged. Different GHSVs were adopted by changing the volumes of catalysts. The concentrations of NO and NO_2 in the inlet and outlet gas were measured by an online chemiluminescence NO−NO_2−NO_x analyzer (42i-HL, Thermo Electron Corp.). Data were recorded after the reactions reached a steady state.

Materials Characterization. TEM, high-resolution transmission electron microscopy (HRTEM), and dark-field scanning transmission electron microscopy (STEM) studies and energy-dispersive X-ray spectroscopy (EDX) mapping were conducted on a JEM 2100F transmission electron microscope. SXRD patterns were obtained at BL14B of the Shanghai Synchrotron Radiation Facility (SSRF) at a wavelength of 1.2398 Å. XPS analysis was undertaken on a Kratos Axis Ultra-DLD system with a charge neutralizer and a 150 W Al (Mono) X-ray gun (1486.6 eV) with a delay-line detector (DLD). The binding energy of the samples was calibrated according to C 1s XPS at a binding energy of 284.6 eV. Curve fitting was carried out by use of XPSPEAK 4.1 with a Shirley background. H_2-TPR experiments were performed on a 2920 adsorption instrument (Micromeritics) with a thermal conductivity detector (TCD) to monitor the consumed H_2. H_2-TPR was conducted at 10 °C·min^{-1} in a 50 mL·min^{-1} flow of 5 vol % H_2 in Ar.

Theoretical Calculations. The structures of the HWO (100) surface, before and after Ce loading by adding ∼15 Å vacuum, were optimized by the Vienna ab initio simulation package (VASP). Density functional theory (DFT) calculations were performed in the whole calculation process. General gradient approximation (GGA) pseudopotentials were used to express the exchange and correlation effects, and pseudopotentials of the projector augmented wave method were used to describe interactions between the core and valence electrons. The energy cutoff for the plane waves was set to 450 eV. The *k*-point sampling was generated with a 2 × 4 × 1 Monkhorst−Pack grid. Lattice constants of the conventional hexagonal HWO cell with space group *P6/mmm* and the three-dimensional (3D) periodic-slab model of HWO (100) surface before and after Ce addition are 7.319 Å × 7.319 Å × 3.881 Å, 14.924 Å × 7.456 Å × 26.482 Å, and 15.057 Å × 7.419 Å × 26.698 Å by optimizing geometries, respectively.

RESULTS AND DISCUSSION

The catalytic activities of CeO_2, supported CeO_2 catalysts, and corresponding supports were tested under the same conditions. A high GHSV of 300 000 h^{-1} was adopted to distinguish the catalytic activities. The NO conversions (X_{NO}) at 300 °C are shown in Figure 1a, and the X_{NO} values as a function of reaction temperature are shown in Figure S1. CeO_2 and three supports give only very low X_{NO}, whereas the SCR activities of supported CeO_2 catalysts are obviously enhanced. The catalytic activities follow the sequence CeO_2/HWO > CeO_2/TiO_2 > CeO_2/Al_2O_3. The reaction kinetics of SCR over CeO_2/Al_2O_3, CeO_2/TiO_2, and CeO_2/HWO were studied at low X_{NO}, and the steady-state reaction rates are shown in an Arrhenius plot (Figure 1b). The apparent activation energy (E_a) for CeO_2/HWO is ∼48 kJ·mol^{-1}, slightly lower than that (50 kJ·mol^{-1}) for CeO_2/TiO_2, whereas the pre-exponential factor for CeO_2/HWO is 3.5 × 10^6 s^{-1}, larger than the corresponding value (2.7 × 10^6 s^{-1}) for CeO_2/TiO_2 (Table S1). A significantly smaller pre-exponential factor for CeO_2/Al_2O_3 gives a good explanation for its low activity although it has a low activation energy.

According to the well-established reaction mechanisms that involve commercial V_2O_5-based catalysts,[23,24] two important cycles, acid-site and redox cycles, are involved in SCR. These cycles almost simultaneously occur on the adjacent dual sites of HO−V−O−V═O (V−OH is a Brønsted acid site and V═O is responsible for activation of NH_3) for NH_3 adsorption and

DOI: 10.1021/acs.est.6b04050
Environ. Sci. Technol. 2017, 51, 473−478

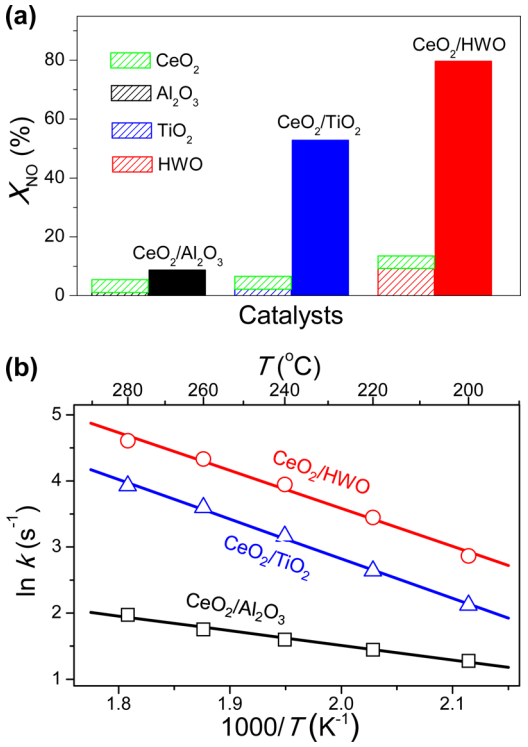

Figure 1. (a) X_{NO} over three CeO_2-based catalysts together with their supports and pure CeO_2. Reaction conditions: 300 °C, 500 ppm of NO, 500 ppm of NH_3, 3 vol % O_2, balance N_2, and GHSV 300 000 h^{-1}. (b) Arrhenius plot for CeO_2/Al_2O_3, CeO_2/TiO_2, and CeO_2/HWO in SCR.

activation.[25,26] Presumably, such adjacent dual sites are present at the periphery of the interface between CeO_2–Al_2O_3 or CeO_2–HWO, because CeO_2 has redox property and both Al_2O_3 and HWO are acidic supports. The presence of adjacent dual sites may partly explain the higher activity of CeO_2/Al_2O_3 and CeO_2/HWO compared with CeO_2 alone. Although TiO_2 normally has fewer Brønsted acid sites on its surface, CeO_2/TiO_2 is even more active than CeO_2/Al_2O_3, indicating that the redox property may be indispensable to reach high activity in SCR.

Figure 2 shows the SXRD patterns of the samples. The diffraction of Al_2O_3, TiO_2, and HWO can be readily indexed to corundum, hexagonal, and anatase structures, respectively. When 12 wt % CeO_2 is loaded, the structures of supports are almost preserved. The weak reflection assigned to crystalline CeO_2 can be discerned for both CeO_2/Al_2O_3 and CeO_2/HWO, and the CeO_2 nanoparticles of CeO_2/HWO are smaller than those of CeO_2/Al_2O_3 because the latter has relatively stronger peaks due to CeO_2 (insets, Figure 2). This implies the presence of strong CeO_2–HWO interactions. Moreover, the size of CeO_2 on TiO_2 is slightly bigger than that of CeO_2 on Al_2O_3 according to the intensity of CeO_2 in the SXRD patterns. Thus, the dispersion of CeO_2 nanoparticles is much easier on acidic supports than on basic supports.[11,27]

Figure 3 shows TEM and HRTEM images of supported CeO_2 catalysts. CeO_2 nanoparticles, with a sub-10 nm size, are highly dispersed on Al_2O_3 (Figure 3a,b).[12] However, CeO_2 nanoparticles with sizes larger than 10 nm can be observed on TiO_2 (Figure 3c,d). By comparison of the TEM images of HWO (Figure S2) and CeO_2/HWO (Figure 3e), it is relatively difficult to distinguish CeO_2 from HWO (Figure 3e,f) because

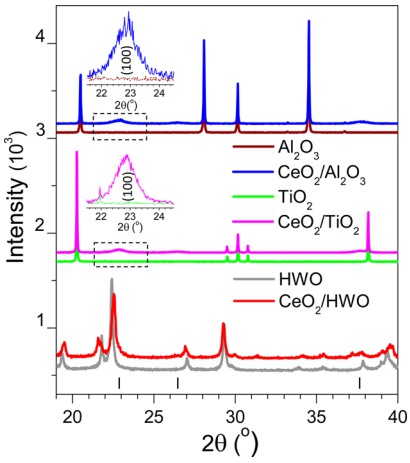

Figure 2. SXRD patterns of CeO_2/Al_2O_3, CeO_2/TiO_2, and CeO_2/HWO with their supports. Short vertical lines show the possible Bragg positions of CeO_2 diffraction.

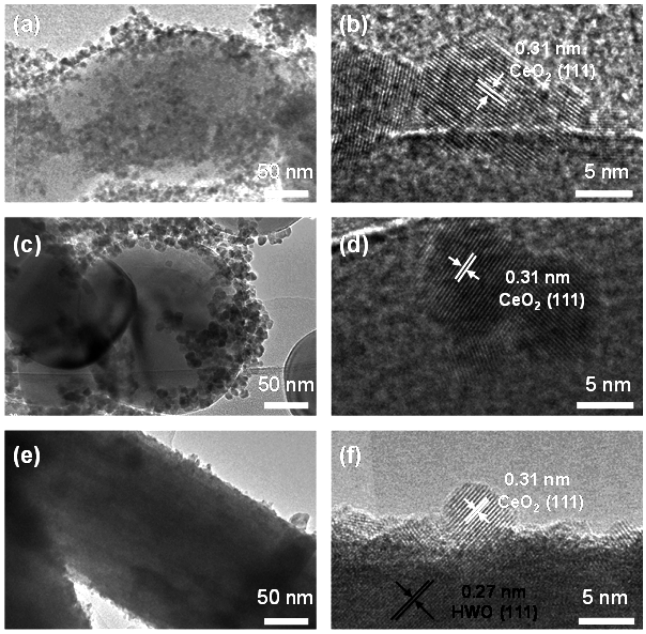

Figure 3. TEM and HRTEM images of (a, b) CeO_2/Al_2O_3, (c, d) CeO_2/TiO_2, and (e, f) CeO_2/HWO.

the atomic number of Ce is only slightly smaller than that of W. According to EDX mapping (Figure S3), the Ce species are highly dispersed on HWO nanorods. In the HRTEM images of Figure 3, fringes with a separation distance of ~0.31 nm are observed in three samples, which can be ascribed to the CeO_2(111) planes. Although the Ce species are also highly dispersed on TiO_2 and Al_2O_3 (Figures S4 and S5), it is clear that the CeO_2 nanoparticles supported on acidic Al_2O_3 and HWO are smaller than those on TiO_2, indicating that supports with abundant Brønsted sites make basic CeO_2 nanoparticles highly dispersed on the surfaces through acid–base interactions. In contrast, bigger CeO_2 nanoparticles are formed on basic TiO_2 support due to the absence of acid–base interactions.[28]

The electronic states of the catalysts were studied by XPS. For nonreducible Al_2O_3 support, there is no strong CeO_2–Al_2O_3 interaction because no distinct shift is observed in the Al 2p XPS before and after CeO_2 loading (Figure S6). Note that

DOI: 10.1021/acs.est.6b04050
Environ. Sci. Technol. 2017, 51, 473–478

for reducible HWO and TiO_2, the supported CeO_2 significantly changes the electronic states of the surface W and Ti species. According to curve-fitting of the XPS data, ~9% of surface W^{6+} species transform into W^{5+} species when CeO_2 is loaded onto HWO (Figure 4a). Likewise, when CeO_2 is loaded onto TiO_2,

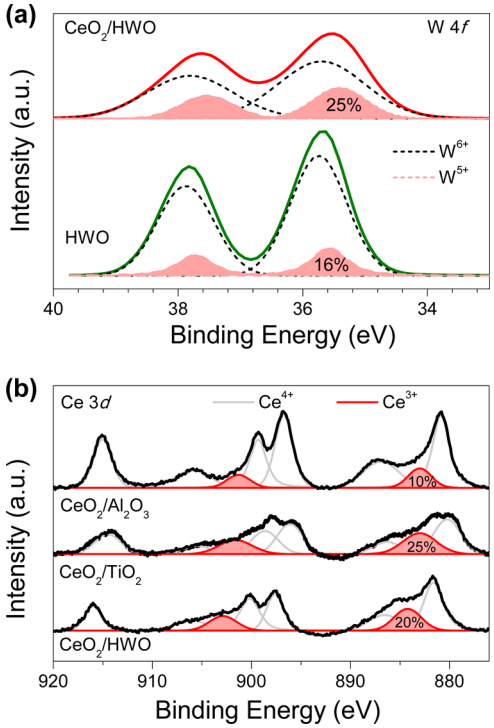

Figure 4. (a) W 4f XPS of HWO and CeO_2/HWO and (b) Ce 3d XPS of the catalysts.

~50% of surface Ti^{4+} on TiO_2 transform into Ti^{3+} (Figure S7). These results demonstrate that the redox properties of HWO and TiO_2 induce strong CeO_2–support interactions.

The Ce 3d XPS data for CeO_2/Al_2O_3, CeO_2/HWO, and CeO_2/TiO_2 are shown in Figure 4b, and curve-fitting was applied to calculate the surface $Ce^{3+}/(Ce^{4+} + Ce^{3+})$ ratio (R_{Ce}^{3+}). R_{Ce}^{3+} of CeO_2/Al_2O_3 is ~10%, whereas the R_{Ce}^{3+} values of CeO_2/HWO and CeO_2/TiO_2 are ~20% and ~25%, respectively, implying that the CeO_2–support interactions of the latter two catalysts are stronger. When it is considered that the CeO_2–Al_2O_3 interaction is weak, the presence of a small portion of Ce^{3+} on CeO_2/Al_2O_3 may be due to the presence of some surface defects. For CeO_2/TiO_2, in view of the presence of a significant amount of Ti^{3+} on the surfaces (Figure S7) and the basic medium during the preparation, the high R_{Ce}^{3+} value might imply the formation of $CeTiO_3$,[29] which can provide the catalytically active Ce–O–Ti structure for SCR.[19] As for CeO_2/HWO, the high R_{Ce}^{3+} value is beneficial for enhancement of the redox ability[30] and thereby the SCR activity.[18]

The reducibility of the catalysts was investigated by H_2-TPR (Figure 5). In the temperature range 250–450 °C, no reduction peak is observed in the H_2-TPR profile of Al_2O_3. An onset of the weak reduction peaks of TiO_2 can be discerned at ~320 °C. The reduction peaks are very weak for CeO_2/Al_2O_3 and CeO_2/TiO_2. A weak peak at ~330 °C appears in the CeO_2 profile, and a very strong reduction peak of the HWO support starts at the same reduction temperature of ~330 °C, which shifts down to a low-onset temperature of ~260 °C for

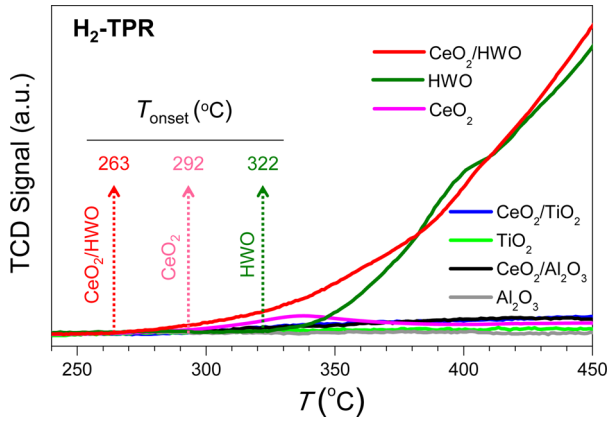

Figure 5. H_2-TPR profiles of supported CeO_2 catalysts together with their supports and pure CeO_2. The onset temperatures (T_{onset}) of CeO_2/HWO, CeO_2, and HWO are also shown.

CeO_2/HWO, indicating the surface oxygen species of CeO_2/HWO have a strong redox ability at low temperatures. The downshift of the low-temperature reduction peak might be mainly ascribed to surface oxygen species of the Ce–O–W structure, which play an important role in SCR. Janssen et al.[23] used labeled oxygen to verify that lattice oxygen participates in the SCR reaction through a reduction/oxidation mechanism over traditional V_2O_5-based catalysts, and Topsøe reported similar results,[25] which can be applicable to current CeO_2/HWO catalysts.[21] Often, redox ability is closely associated with SCR activity, and the stronger the redox ability, the higher the SCR activity.[31] Possibly, the low-temperature redox property of CeO_2/HWO accounts for its high catalytic reactivity at low temperature, leading to the highest catalytic activity among the three CeO_2-based catalysts.

As for supported metal oxide catalysts, it was reported that surface A–O–S bridging bonds are intimately associated with catalytic performance (A and S represent cations of active components and supports, respectively).[32−35] The highest catalytic performance of CeO_2/HWO might originate from the number and activation ability of Ce–O–W bridging bonds, because CeO_2/HWO possesses smaller CeO_2 nanoparticles (Figures 2 and 3) and higher reducible properties (Figure 5). Essentially, the electronic states of Ce–O–W structure are closely related to its activity. Hence, we carried out theoretical calculations based on the DFT method. The electronic density difference contours of Ce–O–W structure motif on HWO (100) and HWO (001) planes are depicted in Figure 6a. The electronic density of Ce overlaps with that of O in the Ce–O–W structure motif, indicating the presence of electronic interactions between CeO_2 and HWO via Ce–O–W bridging bonds. Comparing with the DOS of W and O species of pure HWO support, we found that the Bader charges of both W and O increase after loading of CeO_2 on HWO (Table S2). These results agree fairly well with the XPS data that the amount of W^{5+} species increases and a downshift of the binding energy of O 1*s* orbitals appears after loading of CeO_2 on HWO (Figure S8). In fact, according to a recent report,[19] such an electronic interaction between CeO_2 and reducible supports also exists in CeO_2/TiO_2 via Ce–O–Ti bridging bonds.

Figure 6b shows the density of states (DOS) of the Ce–O–W structure motif at the periphery of CeO_2–HWO interfaces. The DOS of W 5d, O 2p, and Ce 5d orbitals of the Ce–O–W structure motif appear at the same energy regime, demonstrat-

DOI: 10.1021/acs.est.6b04050
Environ. Sci. Technol. 2017, 51, 473–478

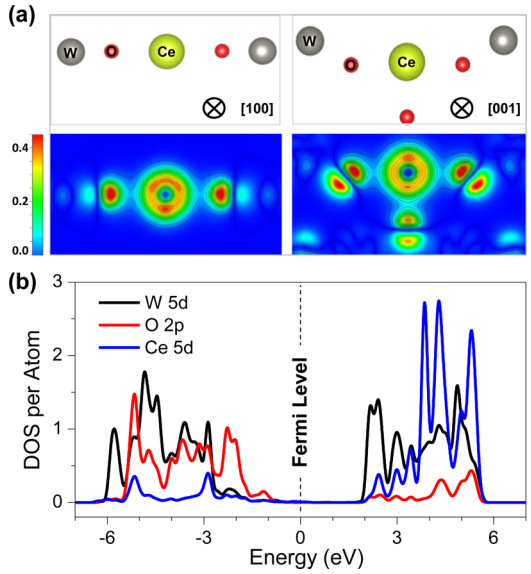

Figure 6. (a) Atom arrangements and corresponding differential charge density contours of HWO (100) and HWO (001) planes. (b) Projected DOS of the Ce−O−W structure motif for CeO_2/HWO.

ing the existence of hybridization of these orbitals to form molecular orbitals. The highest occupied molecular orbital (HOMO) is mainly composed of O 2p and W 5d orbitals, but the lowest unoccupied molecular orbital (LUMO) primarily consists of W 5d and Ce 5d and 4f orbitals (Figure S9).[36] The high DOS of O 2p levels is close in energy to the HOMO, which may readily provide electrons for SCR. As discussed above, there is a redox cycle in SCR, meaning the existence of electron transport between reactants and catalysts. Such electron transport should become much easier on CeO_2/HWO with a very small energy difference among O 2p, Ce 5d and 4f, and W 5d orbitals regardless of the HOMO and LUMO levels. The electronic CeO_2−HWO interactions produce the strong support effect responsible for high SCR activity. Therefore, an increase in CeO_2 loading will increase the number of Ce−O−W structure motifs, thus increasing the SCR activity of CeO_2/HWO, as confirmed in Figure S10, where CeO_2/HWO catalysts give increasingly high X_{NO} over a wide reaction temperature range when the CeO_2 loading reaches 8% in weight or more.

These results demonstrate that, for basic and redox CeO_2 active component, it is suitable to choose supports with acid and redox properties, which are favorable to disperse CeO_2 nanoparticles and to produce a strong support effect via surface Ce−O−M bridging bonds. The support effect originates from two important reactions between active components and supports: (i) acid−base reaction and (ii) redox reaction. The acid−base reaction generally determines the number of surface A−O−S bridging bonds, and the redox reaction governs the activation ability of the surface A−O−S bridging bonds, thus regulating catalytic performance.

For supported metal oxide catalysts, the choice of supports is essentially determined by the acid/base and redox properties of active components. On one hand, for basic metal oxides with redox properties, acid and reducible supports are desirable to enhance catalytic performance. For instance, MnO_x/WO_3 had much higher activity in oxidation reactions than MnO_x/CeO_2.[37] On the other hand, for acidic metal oxides with redox properties, basic and reducible supports should be more suitable. Proft and co-workers[38] studied the support effect of acid VO_x catalysts and found that an increase in activity is observed according to the sequence $VO_x/ZrO_2 > VO_x/TiO_2 > VO_x/Al_2O_3 > VO_x/SiO_2$. Such a support effect originates from the nature of A−O−S structures with different electronic densities.[34,35] Therefore, our results can possibly serve as a general strategy to design and develop efficient supported metal oxide catalysts.

In summary, we chose three representative supports, Al_2O_3, TiO_2, and HWO, according to their acidic properties and redox abilities and systematically studied the support effect of the CeO_2-based catalysts in SCR. The combination of characterization techniques and theoretical calculations demonstrated that Brønsted acidic supports are beneficial for improvement of the dispersed state of CeO_2, besides adsorption of NH_3 reactant in the SCR reaction, and that reducible supports facilitate the formation of the support effect through strong electronic CeO_2−support interactions. Therefore, the largest number and highest activation ability of the Ce−O−W bridging bonds are mainly responsible for the highest catalytic performance caompared with catalysts with an acidic Al_2O_3 or reducible TiO_2 support. This work provides a strategy to design supported metal oxide catalysts by optimizing the support effect.

■ ASSOCIATED CONTENT

Supporting Information

The Supporting Information is available free of charge on the ACS Publications website at DOI: 10.1021/acs.est.6b04050.

Description of calculating the rate constant of SCR; two tables listing pre-exponential factors and activation energies and Bader charges; 10 figures showing X_{NO} vs temperature, TEM image of HWO, STEM images and corresponding EDX mappings; Al 2p and Ti 2p and O 1*s* XPS, projected DOS of Ce-O-W structure motif, and X_{NO} of CeO_2/HWO with different CeO_2 loadings (PDF)

■ AUTHOR INFORMATION

Corresponding Author

*(X.T.) Phone +86-21-65642997; fax +86-21-65643597; e-mail tangxf@fudan.edu.cn.

ORCID

Xingfu Tang: 0000-0002-0746-1294

Author Contributions

§These authors contributed equally to this work.

Notes

The authors declare no competing financial interest.

■ ACKNOWLEDGMENTS

This work was financially supported by the NSFC (21477023) and the STCSM (14JC1400400). The SXRD measurements were conducted at the SSRF.

■ REFERENCES

(1) Finlayson-Pitts, B. J.; Pitts, J. N., Jr. *Atmospheric Chemistry: Fundamentals and Experimental Techniques*; John Wiley and Sons: New York, 1986.

(2) Busca, G.; Lietti, L.; Ramis, G.; Berti, F. Chemical and mechanistic aspects of the selective catalytic reduction of NO_x by ammonia over oxide catalysts: A review. *Appl. Catal., B* **1998**, *18* (1-2), 1−36.

DOI: 10.1021/acs.est.6b04050
Environ. Sci. Technol. 2017, 51, 473−478

(3) Lietti, L.; Nova, I.; Ramis, G.; Dall'Acqua, L.; Busca, G.; Giamello, E.; Forzatti, P.; Bregani, F. Characterization and reactivity of V_2O_5-MoO_3/TiO_2 de-NO_x SCR catalysts. *J. Catal.* **1999**, *187* (2), 419−435.
(4) Granger, P.; Parvulescu, V. I. Catalytic NO_x abatement systems for mobile sources: From three-way to lean burn after-treatment technologies. *Chem. Rev.* **2011**, *111* (5), 3155−3207.
(5) Shan, W.; Liu, F.; Yu, Y.; He, H.; Deng, C.; Zi, X. High-efficiency reduction of NO_x emission from diesel exhaust using a $CeWO_x$ catalyst. *Catal. Commun.* **2015**, *59*, 226−228.
(6) Liu, Z.; Fu, Y.; Tu, J.; Meng, M. Effect of CeO_2 on supported Pd catalyst in the SCR of NO: A DRIFT study. *Catal. Lett.* **2002**, *81* (3−4), 285−291.
(7) Cheng, K.; Liu, J.; Zhang, T.; Li, J.; Zhao, Z.; Wei, Y.; Jiang, G.; Duan, A. Effect of Ce doping of TiO_2 support on NH_3-SCR activity over V_2O_5-WO_3/CeO_2-TiO_2 catalyst. *J. Environ. Sci.* **2014**, *26* (10), 2106−2113.
(8) Zhang, X.; Klabunde, K. Superoxide (O^{2-}) on the surface of heat-treated ceria. Intermediates in the reversible oxygen to oxide transformation. *Inorg. Chem.* **1992**, *31* (9), 1706−1709.
(9) Yao, H. C.; Yao, Y. F. Y. Ceria in automotive exhaust catalysts: I. Oxygen storage. *J. Catal.* **1984**, *86* (2), 254−265.
(10) Gao, X.; Jiang, Y.; Luo, Z.; Fu, Y.; Zhong, Y.; Cen, K. Preparation and characterization of CeO_2/TiO_2 catalysts for selective catalytic reduction of NO with NH_3. *Catal. Commun.* **2010**, *11* (5), 465−469.
(11) Reddy, B. M.; Khan, A. Nanosized CeO_2-SiO_2, CeO_2-TiO_2, and CeO_2-ZrO_2 mixed oxides: Influence of supporting oxide on thermal stability and oxygen storage properties of ceria. *Catal. Surv. Asia* **2005**, *9* (3), 155−171.
(12) Shen, Y.; Zhu, S.; Qiu, T.; Shen, S. A novel catalyst of CeO_2/Al_2O_3 for selective catalytic reduction of NO by NH_3. *Catal. Commun.* **2009**, *11* (1), 20−23.
(13) Peng, Y.; Li, K.; Li, J. Identification of the active sites on CeO_2−WO_3 catalysts for SCR of NO_x with NH_3: An in situ IR and Raman spectroscopy study. *Appl. Catal., B* **2013**, *140−141*, 483−492.
(14) Chen, L.; Li, J.; Ge, M. DRIFT study on cerium-tungsten/titania catalyst for selective catalytic reduction of NO_x with NH_3. *Environ. Sci. Technol.* **2010**, *44* (24), 9590−9596.
(15) Peng, Y.; Li, J.; Chen, L.; Chen, J.; Han, J.; Zhang, H.; Han, W. Alkali metal poisoning of a CeO_2−WO_3 catalyst used in the selective catalytic reduction of NO_x with NH_3: An experimental and theoretical study. *Environ. Sci. Technol.* **2012**, *46* (5), 2864−2869.
(16) Guo, R.; Zhou, Y.; Pan, W.; Hong, J.; Zhen, W.; Jin, Q.; Ding, C.; Guo, S. Effect of preparation methods on the performance of CeO_2/Al_2O_3 catalysts for selective catalytic reduction of NO with NH_3. *J. Ind. Eng. Chem.* **2013**, *19* (6), 2022−2025.
(17) Shan, W.; Liu, F.; He, H.; Shi, X.; Zhang, C. Novel cerium-tungsten mixed oxide catalyst for the selective catalytic reduction of NO_x with NH_3. *Chem. Commun.* **2011**, *47* (28), 8046−8048.
(18) Shan, W.; Geng, Y.; Chen, X.; Huang, N.; Liu, F.; Yang, S. A highly efficient $CeWO_x$ catalyst for the selective catalytic reduction of NO_x with NH_3. *Catal. Sci. Technol.* **2016**, *6* (4), 1195−1200.
(19) Li, P.; Xin, Y.; Li, Q.; Wang, Z.; Zhang, Z.; Zheng, L. Ce-Ti amorphous oxides for selective catalytic reduction of NO with NH_3: Confirmation of Ce-O-Ti active sites. *Environ. Sci. Technol.* **2012**, *46* (17), 9600−9605.
(20) Liu, Z.; Zhang, S.; Li, J.; Ma, L. Promoting effect of MoO_3 on the NO_x reduction by NH_3 over CeO_2/TiO_2 catalyst studied with in situ DRIFTS. *Appl. Catal., B* **2014**, *144*, 90−95.
(21) Chen, L.; Li, J.; Ablikim, W.; Wang, J.; Chang, H.; Ma, L.; Xu, J.; Ge, M.; Arandiyan, H. CeO_2-WO_3 mixed oxides for the selective catalytic reduction of NO_x by NH_3 over a wide temperature range. *Catal. Lett.* **2011**, *141* (12), 1859−1864.
(22) Huang, Z.; Li, H.; Gao, J.; Gu, X.; Zheng, L.; Hu, P.; Xin, Y.; Chen, J.; Chen, Y.; Zhang, Z.; Chen, J.; Tang, X. Alkali- and sulfur-resistant tungsten-based catalysts for NO_x emissions control. *Environ. Sci. Technol.* **2015**, *49* (24), 14460−14465.
(23) Janssen, F. J.; Van den Kerkhof, F. M.; Bosch, H.; Ross, J. R. Mechanism of the reaction of nitric oxide, ammonia, and oxygen over vanadia catalysts. I. The role of oxygen studied by way of isotopic transients under dilute conditions. *J. Phys. Chem.* **1987**, *91* (23), 5921−5927.
(24) Janssen, F. J.; Van den Kerkhof, F. M.; Bosch, H.; Ross, J. R. Mechanism of the reaction of nitric oxide, ammonia, and oxygen over vanadia catalysts. 2. Isotopic transient studies with oxygen-18 and nitrogen-15. *J. Phys. Chem.* **1987**, *91* (27), 6633−6638.
(25) Topsøe, N.-Y. Mechanism of the selective catalytic reduction of nitric oxide by ammonia elucidated by in situ on-line fourier transform infrared spectroscopy. *Science* **1994**, *265*, 1217−1219.
(26) Topsøe, N. Y.; Topsøe, H.; Dumesic, J. A. Vanadia/titania catalysts for selective catalytic reduction (SCR) of nitric-oxide by ammonia: I. Combined temperature-programmed in-situ FTIR and on-line mass-spectroscopy studies. *J. Catal.* **1995**, *151* (1), 226−240.
(27) Reddy, B. M.; Khan, A.; Lakshmanan, P.; Aouine, M.; Loridant, S.; Volta, J. C. Structural characterization of nanosized CeO_2-SiO_2, CeO_2-TiO_2, and CeO_2-ZrO_2 catalysts by XRD, Raman, and HREM techniques. *J. Phys. Chem. B* **2005**, *109* (8), 3355−3363.
(28) Tanaka, K. I.; Ozaki, A. Acid-base properties and catalytic activity of solid surfaces. *J. Catal.* **1967**, *8* (1), 1−7.
(29) Dauscher, A.; Wehrer, P.; Hilaire, L. Influence of the preparation method on the characteristics of TiO_2-CeO_2 supports. *Catal. Lett.* **1992**, *14* (2), 171−183.
(30) Kopelent, R.; van Bokhoven, J. A.; Szlachetko, J.; Edebeli, J.; Paun, C.; Nachtegaal, M.; Safonova, O. V. Catalytically active and spectator Ce^{3+} in ceria-supported metal catalysts. *Angew. Chem., Int. Ed.* **2015**, *54* (30), 8728−8731.
(31) Lietti, L.; Nova, I.; Forzatti, P. Selective catalytic reduction (SCR) of NO by NH_3 over TiO_2-supported V_2O_5-WO_3 and V_2O_5-MoO_3 catalysts. *Top. Catal.* **2000**, *11* (1), 111−122.
(32) Briand, L. E.; Farneth, W. E.; Wachs, I. E. Quantitative determination of the number of active surface sites and the turnover frequencies for methanol oxidation over metal oxide catalysts: I. Fundamentals of the methanol chemisorption technique and application to monolayer supported molybdenum oxide catalysts. *Catal. Today* **2000**, *62* (2), 219−229.
(33) Gao, X.; Wachs, I. E. Molecular engineering of supported vanadium oxide catalysts through support modification. *Top. Catal.* **2002**, *18* (3−4), 243−250.
(34) Banares, M. A.; Wachs, I. E. Molecular structures of supported metal oxide catalysts under different environments. *J. Raman Spectrosc.* **2002**, *33* (5), 359−380.
(35) Keller, D. E.; Airaksinen, S. M.; Krause, A. O.; Weckhuysen, B. M.; Koningsberger, D. C. Atomic XAFS as a tool to probe the reactivity of metal oxide catalysts: Quantifying metal oxide support effects. *J. Am. Chem. Soc.* **2007**, *129* (11), 3189−3197.
(36) Vayssilov, G. N.; Lykhach, Y.; Migani, A.; Staudt, T.; Petrova, G. P.; Tsud, N.; Skála, T.; Bruix, A.; Illas, F.; Prince, K. C.; Matolín, V.; Neyman, K. M.; Libuda, J. Support nanostructure boosts oxygen transfer to catalytically active platinum nanoparticles. *Nat. Mater.* **2011**, *10* (4), 310−315.
(37) Amini, M.; Pourbadiei, B.; Ruberu, T. P. A.; Woo, L. K. Catalytic activity of MnO_x/WO_3 nanoparticles: Synthesis, structure characterization and oxidative degradation of methylene blue. *New J. Chem.* **2014**, *38* (3), 1250−1255.
(38) Fievez, T.; Weckhuysen, B. M.; Geerlings, P.; Proft, F. D. Chemical reactivity indices as a tool for understanding the support-effect in supported metal oxide catalysts. *J. Phys. Chem. C* **2009**, *113* (46), 19905−19912.

DOI: 10.1021/acs.est.6b04050
Environ. Sci. Technol. 2017, 51, 473−478